Macromolecular Materials and Engineering
www.mme-journal.de

# Nanostructured Biopolymer/Few-Layer Graphene Freestanding Films with Enhanced Mechanical and Electrical Properties

*Cláudia Silva, Sofia G. Caridade, Eunice Cunha, Maria P. Sousa, Helena Rocha, João F. Mano, Maria C. Paiva,* and Natália M. Alves**

**In the present work, novel freestanding multilayered films based on chitosan (CHI), alginate (ALG), and functionalized few-layer graphene are developed through layer-by-layer assembly. First, functionalized few-layer graphene aqueous suspensions are prepared from graphite by a stabilizer-assisted liquid phase exfoliation process, using a pyrene derivative as stabilizer. Afterward, the films are produced and their physical, morphological, thermal, and mechanical properties are evaluated. Furthermore, their degradation and swelling profiles, as well as their biological behavior, are assessed. The incorporation of functionalized few-layer graphene results in films with a nanolayered structure, lower roughness than the control CHI/ALG films, and hydrophilic behavior. The mechanical characterization reveals an increase of the Young's modulus, ultimate tensile strength, and elongation at break due to the incorporation of the graphene derivative. A decrease in the electrical resistivity of the multilayered films is also observed. The biological assays reveal improved cytocompatibility toward L929 cells when functionalized few-layer graphene is incorporated in the CHI/ALG matrix. Therefore, these new graphene-reinforced multilayered films exhibit interesting properties and great potential for biomedical applications, particularly in wound healing and cardiac and bone tissue engineering.**

## 1. Introduction

Graphene is a 2D monolayer of $sp^2$-hybridized carbon atoms arranged in a hexagonal lattice with a carbon–carbon bond length of 0.142 nm.[1–3] Graphene properties have been extensively studied since it was first isolated in 2004 by Novoselov et al.[4] It has a great potential for reinforcement in composite materials[4,5] due to its Young's modulus of 1 TPa, intrinsic strength of 130 GPa,[6] room temperature (RT) electron mobility of 250 000 $cm^2\ V^{-1}\ s^{-1}$,[4] and optical transmittance of 97.7%.[7] Other promising application areas for graphene are photonics, optoelectronics, energy generation and storage, sensors for gas detection, and biomedical areas, particularly in biosensing, drug and gene delivery, and tissue engineering.[4] Graphene is a material with hydrophobic behavior and considerable chemical inertia. However, it is highly susceptible to physical adsorption through $\pi$–$\pi$ interactions[1] and it can be chemically functionalized via noncovalent or covalent approaches.[4,8] Moreover, nonfunctionalized graphene sheets may tend to restack, through van der Waals interactions to reform graphite.[9] The functionalization of graphene allows the production of stable aqueous suspensions as well as the enhancement of the interaction between graphene and other materials, which has particular importance for the application of graphene in layer-by-layer (LbL) assembly.[9,10] The noncovalent functionalization through $\pi$–$\pi$ interactions is an effective and nondestructive method that does not affect the chemical structure or the electronic properties of the graphene sheets.[11,12] Stabilizer-assisted liquid phase exfoliation of graphene has been reported using polymers, surfactants, and aromatic compounds as stabilizers, to enhance the interaction with the solvent and prevent restacking of graphene sheets. Polycyclic aromatic hydrocarbons such as pyrene derivatives[13] are promising stabilizers that yield stable suspensions with high graphene content. These compounds adsorb at the graphene surface through $\pi$–$\pi$ interactions, which appear to be stronger than graphene–graphene interactions according to Li et al.[14] Moreover, low concentration pyrene derivative solutions are effective for the preparation of stable suspensions of graphene (or exfoliated graphite, EG), while large concentrations

C. Silva, Dr. S. G. Caridade,[+] Dr. M. P. Sousa,[+] H. Rocha, Prof. J. F. Mano,[+] Dr. N. M. Alves
3B's Research Group, Biomaterials, Biodegradables and Biomimetics
University of Minho
Headquarters of the European Institute of Excellence on Tissue Engineering and Regenerative Medicine
AvePark-Parque de Ciência e Tecnologia
4805-017 Barco, Taipas, Guimarães, Portugal
E-mail: nalves@dep.uminho.pt

C. Silva, Dr. S. G. Caridade, Dr. M. P. Sousa, H. Rocha, Prof. J. F. Mano, Dr. N. M. Alves
ICVS/3B's, Associate PT Government Laboratory
4710-057 Braga/Guimarães, Portugal
E-mail: mcpaiva@dep.uminho.pt

C. Silva, Dr. E. Cunha, H. Rocha, Dr. M. C. Paiva
Institute for Polymers and Composites/i3N
Department of Polymer Engineering
University of Minho
4800-058 Guimarães, Portugal

The ORCID identification number(s) for the author(s) of this article can be found under https://doi.org/10.1002/mame.201700316.

[+]Present address: Department of Chemistry CICECO—Aveiro Institute of Materials, University of Aveiro, 3810-193

**DOI: 10.1002/mame.201700316**

 

of surfactants or polymers are required to achieve a similar effect, as reported by Parviz et al.[13]

Natural polymers are extensively used in biomedical applications due to their inherent biocompatibility and biodegradability.[15] Alginate (ALG) is a natural anionic polymer usually extracted from brown algae. It is a linear copolymer polysaccharide containing blocks of (1,4)-linked β-D-mannuronate (M) and α-L-guluronate (G) residues.[16,17] ALG presents low cost, biocompatibility, low toxicity, and forms hydrogels whose structure is similar to extracellular matrices of living tissues.[16] Chitosan (CHI) is a natural cationic polymer produced through the alkaline deacetylation of chitin, which promotes the hydrolysis and conversion of the acetyl groups of chitin in free amine groups.[18,19] It is a biocompatible, biodegradable, nontoxic polymer with spermicidal, hemostatic, and antibacterial behavior.[20,21] CHI is widely employed in several biomedical areas in the form of gels, films, or fibers.[19,20] One of the major drawbacks of natural polymers is their poor mechanical and electrical properties.[22] The reinforcement of natural polymers with graphene and graphene-based materials has been reported as a solution to overcome this drawback owing to their excellent mechanical and electrical properties. Besides the enhancement of the mechanical and electrical properties of natural polymers, other advantages of using graphene have been reported, such as the increase of cellular attachment and proliferation and the improvement of biosensor's effectiveness.[5,23–26]

LbL assembly is a versatile technique used to modify surfaces and to produce nanostructured polymeric multilayered films through the alternate adsorption of complementary multivalent molecules on a surface, by application on substrates with any geometry. The assembly may be achieved by electrostatic or nonelectrostatic interactions,[27,28] and thus it is not limited to polymeric polyelectrolyte (PE) systems.[27,29] Several works reported the incorporation of peptides, carbon nanotubes, clays, dyes, metal oxides, particles, nucleic acids, proteins, enzymes, DNA, and viruses in multilayered films.[27,30] Several materials can be used and the number of depositions can be controlled, allowing the production of multilayered structures with tailored thickness, chemical composition, structure and properties.[27] LbL structures are produced for application in several fields including biomimetics, sensing and biosensing, drug/gene/therapeutic delivery, protein adsorption, tissue and regenerative medicine, and energy storage and conversion.[27,29] Multilayered films built with graphene-based materials, mainly with graphene oxide (GO) and reduced GO, have been reported by several researchers.[31–39] However, reports on multilayered films built with graphene-based materials and natural polymers are still scarce.[40–42] Tang et al. reported the production and characterization of multilayered films based on GO and regenerated cellulose. The properties of these films were suitable for applications in advanced biochemical and electrochemical devices.[40] Wen and co-workers coated vitreous carbon electrodes with multilayered films based on GO and CHI. The coated electrodes presented excellent electrocatalytic sensing performance for detection of dopamine and uric acid.[41] The development of freestanding (FS) multilayered films based on CHI, ALG, and GO with interesting properties for biomedical applications such as wound healing and tissue engineering of cardiac and bone tissues was also reported.[42] To our knowledge, the LbL assembly of natural polymers and noncovalently functionalized few-layer graphene produced through stabilizer-assisted liquid phase exfoliation was not reported.

The present work reports the development of FS multilayered films using the LbL technique with the composition $(CHI/ALG/CHI/fG(XGC))_{100}$, where functionalized few-layer graphene produced by stabilizer-assisted liquid phase exfoliation is used as filler to reinforce the polymeric composite. The effect of incorporating this type of graphene in multilayered films specifically produced by the LbL methodology was studied. Before the production of the FS multilayered films, quartz crystal microbalance with dissipation (QCM-D) experiments were performed to investigate the best conditions for the film build-up. Three different types of pristine graphite were functionalized to produce few-layer graphene and were characterized by Raman spectroscopy, UV-visible (UV–vis) spectroscopy, thermogravimetric analysis (TGA), and zeta potential (ZP) measurements. The suspension that yielded higher concentration of few layer graphene in suspension and showed superior stability was selected to prepare the FS multilayered films by LbL. Afterward, the FS multilayered films produced were characterized by scanning electron microscopy (SEM), atomic force microscopy (AFM), TGA, and Raman Spectroscopy. The mechanical performance, wettability, water uptake (WU), degradation, and biological behavior of the obtained films were also evaluated.

## 2. Results and Discussion

### 2.1. Synthesis and Characterization of Functionalized Few-Layer Graphene

#### *2.1.1. Synthesis of Functionalized Few-Layer Graphene*

The aqueous suspensions of functionalized few-layer graphene were prepared through stabilizer-assisted liquid phase exfoliation, a noncovalent functionalization approach. Suspensions of three different graphite products, fG(Micrograf), fG(Graphexel), and fG(XGC) were produced. The pyrene derivative (PY) used to produce the few-layer graphene aqueous suspensions is represented in **Figure 1**. The suspensions were prepared by sonication of the selected graphite materials in $5 \times 10^{-5}$ M PY solutions. After centrifugation, the supernatant was collected, characterized, and tested for possible application using the LbL technique.

#### *2.1.2. Characterization of Functionalized Few-Layer Graphene*

*Raman Spectroscopy*: Raman Spectroscopy has been extensively used to study carbon materials such as graphense,

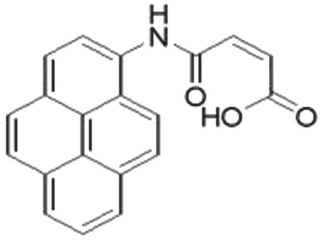


**Figure 1.** Pyrene derivative molecular structure.

pyrolytic graphite, and carbon nanotubes, providing relevant information about chemical and structural characteristics of these materials. The pristine graphite materials used and the derivatives obtained by liquid phase exfoliation were characterized by Raman spectroscopy and their spectra are presented in **Figure 2**a–c. The Raman spectra of PY, pristine graphite (Micrograf, Graphexel and XGC), and the exfoliated materials obtained from fG(Micrograph), fG(Graphexel), and fG(XGC) show three major bands characteristic of $sp^2$ carbon materials. The D band, near 1350 $cm^{-1}$, is related to the presence of structural defects in the hexagonal $sp^2$ carbon lattice of graphene and with edge effects.[43,44] The G band, at ≈1580 $cm^{-1}$, is associated with the doubly degenerate phonon mode at the Brillouin zone center, and it is related with the in-plane vibration of the $sp^2$ carbon atoms.[43] The relative signal intensity of the D band to the G band ($I_D/I_G$) provides information about the level of "disorder" in terms of covalent modification of the graphene structure.[44,45] The band near 2700 $cm^{-1}$, designated as 2D band, has nearly the double frequency of the D band and is due to a second order Raman scattering process.[44] The number of layers for *n*-layer graphene can be estimated by analyzing the shape, width, and position of the 2D band. Ferrari et al. reported that an increase in the number of layers originates a broader 2D band shifted to higher wavenumber.[44,46] In pristine graphite, the 2D band consists of two components and appears at ≈2720 $cm^{-1}$[47] while graphene presents a single sharp peak centered at a wavenumber lower than 2700 $cm^{-1}$.[45]

The analysis of the Raman spectra in Figure 2a shows an increase of the $I_D/I_G$ ratio for the fG(Micrograf) relative to Micrograf (pristine), from 0.20 to 0.47. According to Parviz et al., this may be a consequence of a decrease in the flake size when Micrograf (pristine) in aqueous suspension was exposed to sonication, to produce fG(Micrograf). As the flake size decreases, the extension of exposed edges per flake area increases, resulting in the intensity increase of the D band relative to the G band,[13] particularly if edges with armchair configuration were formed.[45] Moreover, the 2D band in fG(Micrograf) is downshifted to a lower wavenumber which indicates that the exfoliation was successfully achieved. The position, near 2707 $cm^{-1}$, and symmetric shape of the 2D band in fG(Micrograf) confirm the few-layer nature of the functionalized graphene obtained from pristine Micrograf. The small peaks observed at ≈1400 and 1620 $cm^{-1}$ are characteristic of PY.[48] The Raman spectrum of fG(Graphexel) presented in Figure 2b also depicts the characteristic peaks of PY near 1400 and 1620 $cm^{-1}$, as well as an increase of the $I_D/I_G$ band ratio relative to the pristine material from 0.03 to 0.20. The 2D band shift toward lower wavenumber and a change in peak shape was observed indicating the successful exfoliation of pristine Graphexel. Finally, XGC (pristine) and fG(XGC) do not show significant differences in the Raman spectra, Figure 2c, owing to the structural similarity of the pristine and functionalized materials. The pristine XGC is already partially oxidized and exfoliated, formed by small flakes (and thus a large extension of edge carbons), resulting on a high intensity D band.[13] No significant changes in $I_D/I_G$ were observed after the functionalization process. The position of the 2D band along with its symmetric shape reveals the few-layer nature of fG(XGC).

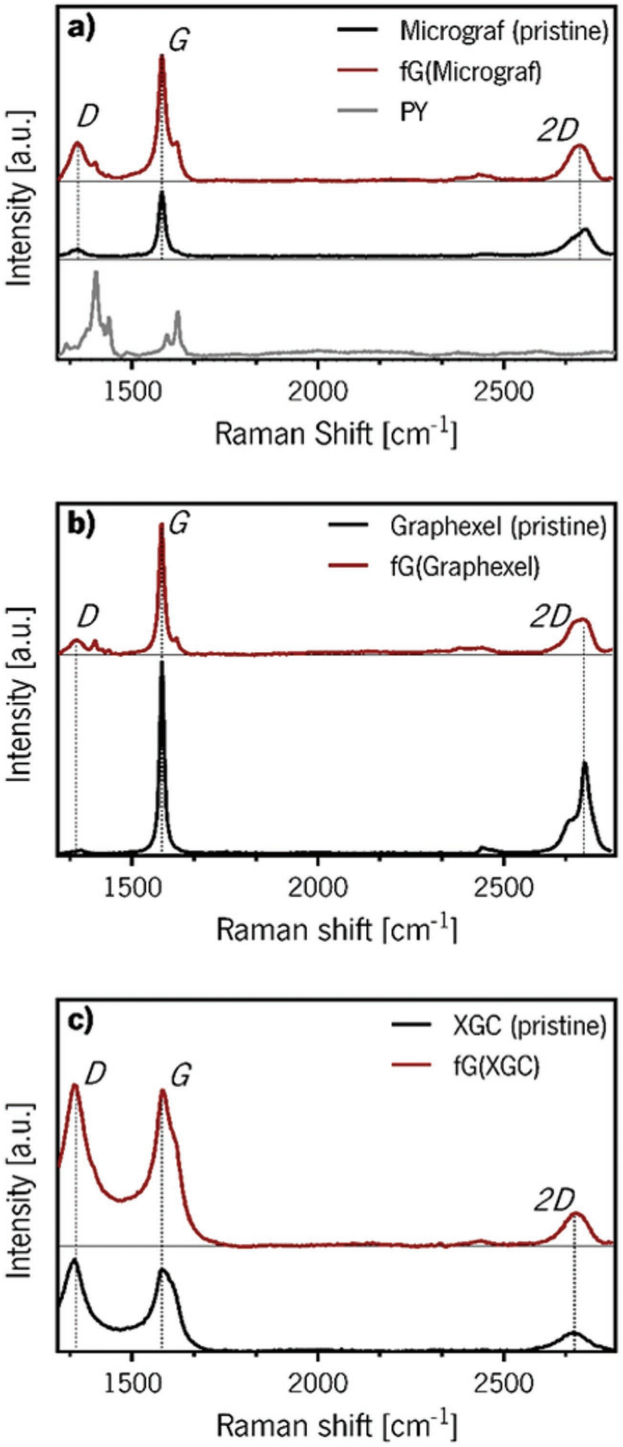


**Figure 2.** Raman spectra of a) PY, Micrograf (pristine), and fG(Micrograf); b) Graphexel (pristine) and fG(Graphexel); and c) XGC (pristine) and fG(XGC).

*Ultraviolet-Visible Spectroscopy*: The UV–vis spectra of PY solution and aqueous suspensions of functionalized few-layer graphene are presented in **Figure 3**. The concentration of the suspensions of functionalized graphene was determined using the Lambert–Beer Law equation, considering the absorptivity

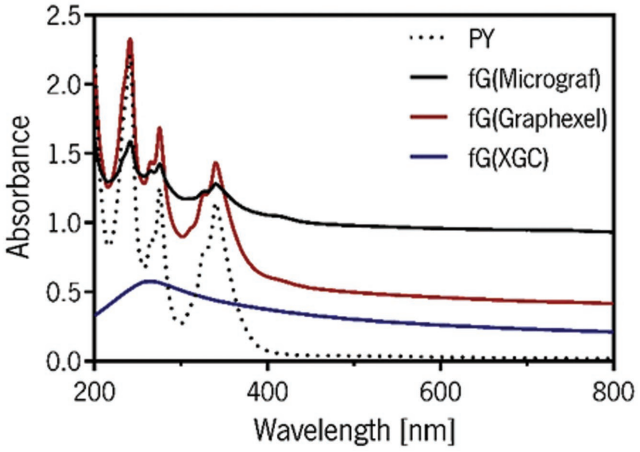


**Figure 3.** UV–vis spectra of PY, fG(Micrograf), fG(Graphexel), and fG(XGC).

coefficient of 2460 $dm^3\ g^{-1}\ m^{-1}$ at 660 nm, as reported by Viinikanoja et al.[49] Figure 3 shows that the UV–vis spectra of fG(Micrograf) and fG(Graphexel) were modulated by the spectra of PY, corroborating the results of previous works describing typical spectra of PY-functionalized few-layer graphene aqueous suspensions.[49,50] Conversely, the spectrum of fG(XGC) was observed to be similar to the spectrum of GO,[9] possibly owing to the partially oxidized nature of XGC (pristine), with a maximum absorbance near 265 nm attributed to $\pi \rightarrow \pi^*$ transitions of the conjugated C—C bonds.[51] It should be noticed that the UV–vis spectrum presented for fG(XGC) was obtained for the 10x diluted suspension since the concentration of the as-produced suspension was too high. The spectra of fG(Micrograph) and fG(Graphexel) were obtained for the as-produced suspensions.

The concentration of the functionalized few-layer graphene suspensions produced is presented in **Table 1** as well as the yield of the functionalization process. Table 1 shows that fG(XGC) yields highly concentrated aqueous suspensions, probably due to its smaller flake size that facilitates the PY intercalation and the exfoliation of the graphene layers. This is important for the production of FS multilayered films by LbL that requires the availability of a large volume of stable solutions of polyelectrolytes with a concentration near 0.25 mg $mL^{-1}$.

*Thermogravimetric Analysis*: The TGA results obtained for the pristine and functionalized graphite materials, and for the PY used in the functionalization process, are presented in **Figure 4**.

**Table 1.** Initial concentration of the pristine graphite materials (Micrograf, Graphexel, and XGC), concentration of the functionalized graphite materials (fG(Micrograf), fG(Graphexel), and fG(XGC)) in aqueous suspension, and % yield of the functionalization process.

| Suspension | Initial concentration of pristine material [mg $cm^{-3}$] | Concentration of few-layer graphene in suspension [mg $cm^{-3}$] | Yield [%] |
|---|---|---|---|
| fG(Micrograf) | 1.000 | 0.039 | 3.900 |
| fG(Graphexel) | 1.000 | 0.018 | 1.800 |
| fG(XGC) | 1.000 | 0.246 | 24.60 |

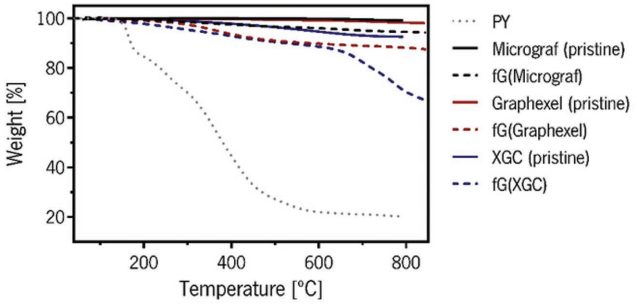


**Figure 4.** TGA thermograms of PY, fG(Micrograf), fG(Graphexel), and fG(XGC).

PY shows the lowest thermal stability, starting thermal degradation above ≈150 °C. The weight loss observed for the pristine graphite materials is small and mainly due to the release of adsorbed water and residual oxidation, as reported by Parviz et al.[13] The pristine Micrograf and Graphexel are thermally stable across the temperature range analyzed, while XGC, formed by smaller and partially oxidized flakes, registered a weight loss of 7.4 wt% at 800 °C, starting above 300 °C. After functionalization with PY the thermal stability decreases above 300 °C for fG(Micrograf) and fG(Graphexel), reaching a weight loss of 5.50 and 11.9 wt%, respectively, at 800 °C. The thermal stability of fG(Graphexel) and fG(XGC) is comparable up to 600 °C. The results demonstrate the extensive functionalization of the graphite materials with PY.

*Zeta Potential*: The stability of the functionalized few-layer graphene aqueous suspensions was assessed through ZP measurements. **Table 2** presents the results obtained for the suspensions at pH = 7. The value for a PY aqueous solution is also included for the sake of comparison. The results show that all the suspensions are characterized by a negative ZP at this pH, which is related with the deprotonation of the carboxylic acid groups of PY adsorbed at the few-layer graphene surface.[9,52] According to the literature, particles with ZP more positive than +30 mV or more negative than −30 mV are considered to form stable suspensions owing to the strong electrostatic repulsion between them.[52] Thus, it is expected that fG(Micrograf), fG(Graphexel), and fG(XGC) form stable aqueous suspensions at pH = 7.

### 2.2. Real-Time Monitoring of the Multilayered Film Production by QCM-D

The fG(XGC) aqueous suspension was selected for the preparation of FS multilayered films accounting for its stability and yield of exfoliation. QCM-D was used to validate the production

**Table 2.** ZP of fG(Micrograf), fG(Graphexel), fG(XGC), and PY.

| | |
|---|---|
| fG(Micrograf) | −31 ± 2 mV |
| fG(Graphexel) | −32 ± 2 mV |
| fG(XGC) | −35 ± 1 mV |
| PY | −14 ± 1 mV |

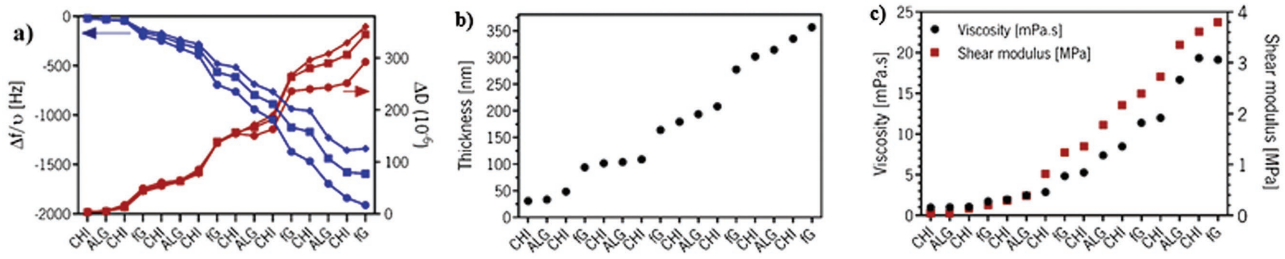


**Figure 5.** a) Normalized frequency ($\Delta f/\upsilon$) and dissipation ($\Delta D$) changes measured by QCM-D during the build-up of $(CHI/ALG/CHI/fG(XGC)_4$. The data for the 3rd (●), 5th (■), and 7th (◆) overtones are presented. (b) Thickness and c) viscosity (●) and shear modulus (■) of the growing $(CHI/ALG/CHI/fG(XGC)_4$ film as a function of the layers deposited calculated with the Voigt-based model.

of the multilayered films based on the chosen polymers and fG(XGC).

**Figure 5**a shows the build-up of $(CHI/ALG/CHI/fG(XGC))_4$ using QCM-D. A decrease of $\Delta f$ with the injection of CHI, ALG, and fG(XGC) was detected, indicating that mass was added to the system during each deposition step. Therefore, the LbL assembly of the polyelectrolytes and fG(XGC) suspension was successful. The $\Delta f$ decay observed for each deposition step is different for the three overtones represented, meaning that the adsorbed layers do not obey to the Sauerbrey equation. This may originate on the viscoelastic behavior of the adsorbed film and with a nonhomogeneous deposition of the film along the crystal surface. Regarding $\Delta D$, an increase was observed after each CHI, ALG, and fG(XGC) deposition owing to the viscoelastic nature of the adsorbed layers.

The viscoelastic properties of the produced films were estimated by applying a Voigt-based model. Assuming $\rho_B = 1.0$ g cm$^{-3}$, $\eta_B = 1$ mP s, and a fixed density of the layer $\rho_L = 1.4$ g cm$^{-3}$. The thickness of the films was estimated as a function of the number of layers. Figure 5b shows that the film thickness increased with the number of layers, the deposition of fG(XGC) being the major driver of this effect, revealing a strong interaction between fG(XGC) and CHI. A value of ≈357 nm for the overall thickness was estimated, based on the assumption that the adsorbed layer has a uniform thickness.

The viscosity and the shear modulus were estimated under the same assumptions used for thickness. Figure 5c reveals an increase on both properties during the build-up of the film, as already reported in other studies related with the deposition of viscoelastic films.[53–55]

Based on the QCM-D results, two types of multilayered films with different compositions were produced, $(CHI/ALG/CHI/ALG)_{100}$ used as control and $(CHI/ALG/CHI/fG(XGC))_{100}$, both with 100 tetralayers and a thickness of ≈50 µm, as explained at the Experimental Section.

### 2.3. Characterization of the Freestanding Multilayered Films

#### *2.3.1. Raman Spectroscopy*

Raman spectroscopy was used to detect the incorporation of fG(XGC) along the FS multilayered films as well as to analyze its distribution over the polymeric films. The Raman spectra presented in **Figure 6**a confirm the incorporation of fG(XGC) in the FS multilayered films, monitoring the presence of the characteristic D, G, and 2D bands of the graphene-based material, that are absent in the control films. The mapping of the nanoparticles distribution was carried out by calculating the integrated intensity over the spectral range of 1500–1700 cm$^{-1}$

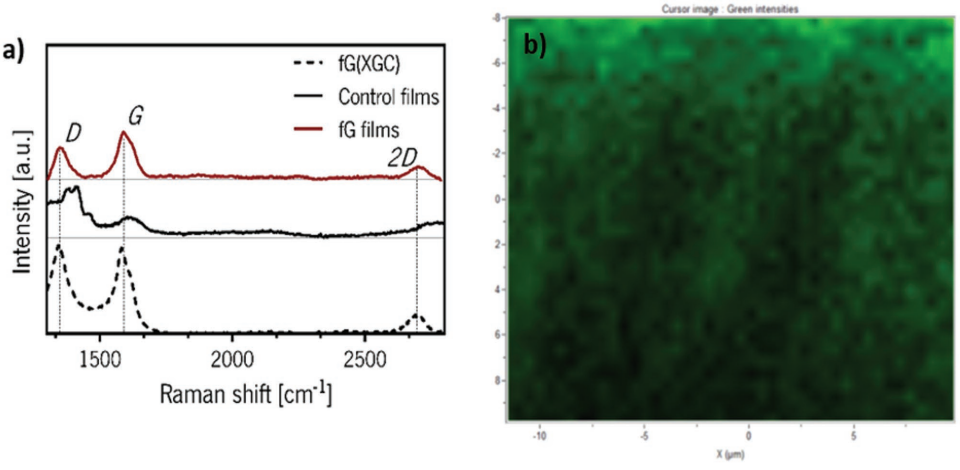


**Figure 6.** a) Raman spectra of fG(XGC), control films, and fG films. b) Distribution of fG(XGC) along the (CHI/ALG) film observed by Raman spectroscopy (the map was built based on the calculated area of the G band of the graphite material; the green spots in the Raman mapping correspond to large G band areas, while the black spots correspond to a G band area near zero).

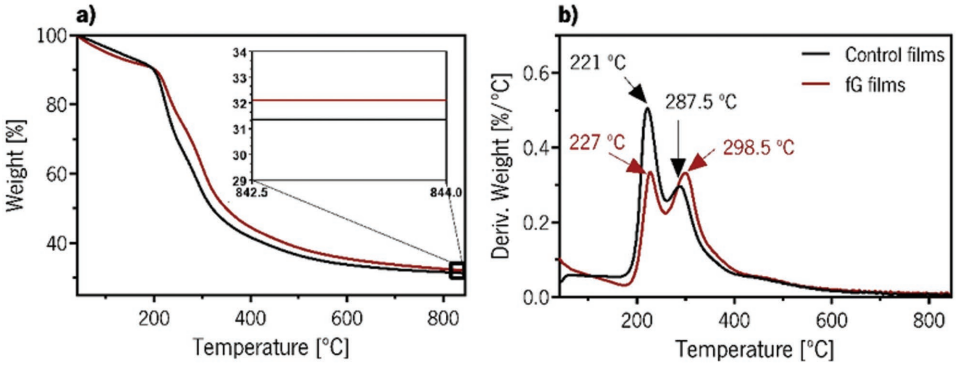


**Figure 7.** a) TGA curves obtained for the FS multilayered films (control and fG), with inset showing a magnification for the temperature range of 842.5–844.0 °C, and b) derivative of the weight loss curves (DTGA) for both FS multilayered films, as a function of temperature (°C).

(G band). The green color intensity correlates to the concentration of fG(XGC) in the polymeric FS multilayered films. Figure 6b illustrates a continuous and uniform distribution of fG(XGC) along the FS multilayered films.

### 2.3.2. Thermogravimetric Analysis

The thermal stability of the control and fG FS multilayered films was evaluated by TGA, and the weight percentage of functionalized few-layer graphene incorporated in the multilayered films was determined. The results, illustrated in **Figure 7**a,b, indicate that both multilayered films have similar thermal stability when heated up to 845 °C under inert atmosphere, with a slightly higher stability of the fG FS multilayered relative to the control films above 200 °C. The initial weight loss below 200 °C is mostly due to the release of strongly adsorbed water (≈10 wt%), which is not considerably affected by the fG presence. The major weight loss is observed between 200 and 400 °C, due to the decomposition of the polymeric materials and the PY used for the XGC functionalization. A similar result was observed by Wang et al.[56] and He et al.[57] for composites based on CHI and graphene derivatives and by Ionita et al.[58] and Nie et al.[59] for ALG/graphene derivatives composites. Above 600 °C, the weight loss tends to stabilize, leaving a residual weight of carbonaceous material from the polymer carbon backbone, for the control films, and also from the graphene-based material, for the fG FS multilayered films. The latter originate a slightly higher residual weight compared to the control films since the graphene-based material fraction has a high thermal stability under inert atmosphere. The residual weight of the control and fG multilayered films was 31.4% and 32.1 wt%, respectively. Considering also that the residue of fG(XGC) at 845 °C was ≈66.9 wt%, a weight content of ≈1.04 wt% of fG(XGC) in the FS multilayered films was estimated.

### 2.3.3. Scanning Electron Microscopy

The morphology of the surface of the upper side (facing outward) and cross-section of the fG and control films was analyzed at the micrometer scale by SEM, as depicted in **Figure 8**. This figure includes a representative photograph of both fG and control FS films, to illustrate their macroscopic morphology.

Regarding the surface morphology, no significant differences were found between the control, Figure 8a1, and fG films, Figure 8b1. In general, at the microscale, both control and fG FS multilayered films revealed a uniform morphology. Previous work on the preparation of CHI/ALG multilayered films showed a similar surface morphology to that obtained in the present work for the control films.[60–62] The cross-section of the FS multilayered films depicted in Figure 8a2,b2 shows a dense structure for both nanocomposite films, indicating a strong interaction between CHI and fG(XGC), comparable to CHI/ALG interaction. This is expected to contribute positively to the FS film mechanical properties. Dense structures obtained by LbL were reported before by other authors.[62,63]

### 2.3.4. Atomic Force Microscopy

The 2D and 3D surface topographies of the FS multilayered films, imaged by AFM, are represented in **Figure 9**b,c. The root-mean-square values of the surface roughness, $R_{RMS}$, for the region represented in Figure 9c1,c2 are presented in Figure 9a.

A decrease in the $R_{RMS}$ from 195 ± 2 to 140 ± 30 nm was observed with the incorporation of fG(XGC) in the FS multilayered films, opposing to the reported effect of GO incorporation in CHI/ALG FS multilayered films prepared by a similar process.[42] This dissimilarity may be associated to the flat topography characteristic of graphene-based materials. Figure 9b shows the average height values, $H_{AV}$, of control and fG FS multilayered films. The $H_{AV}$ values measured are near $R_{RMS}$ which indicates a considerably uniform topography along the FS multilayered films.

### 2.3.5. Water Contact Angle

The wettability of the FS multilayered films was evaluated by water contact angle analysis (WCA) measurements. **Figure 10** shows the hydrophobic character of the control films presenting a WCA near 111°. Similar results were reported by Silva et al. for CHI/ALG FS multilayered films.[61] The incorporation of fG decreased the WCA to ≈86°. Such behavior was reported in a

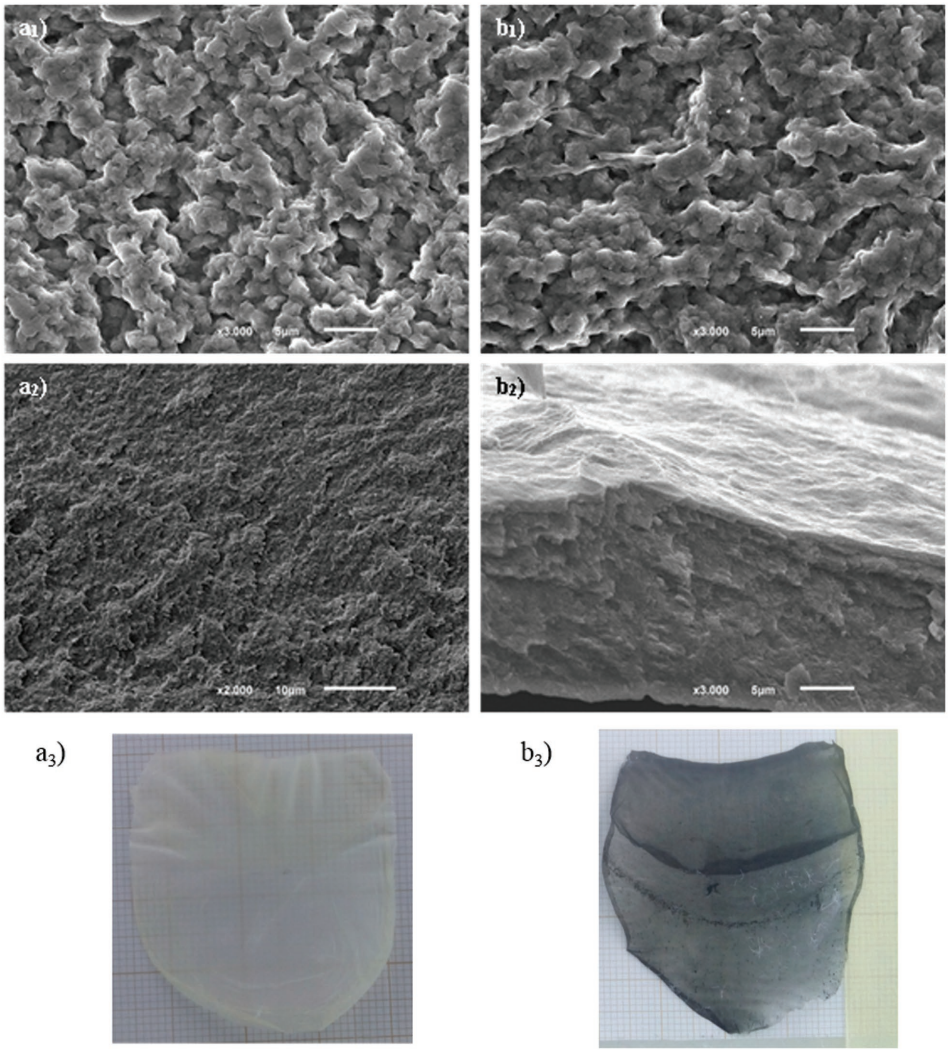


**Figure 8.** SEM images of $a_1$) surface and $a_2$) cross-section of control films; $b_1$) surface and $b_2$) cross-section of fG films; photographs of $a_3$) control films and $b_3$) fG films.

previous work[42] for FS multilayered films incorporating other forms of functionalized graphene. The hydrophobic character of graphene may be tuned by chemical modification (oxidation, covalent or noncovalent functionalization) inducing a hydrophilic character.[64] In the present work, the hydrophilic character of the fG(XGC) in suspension is due to the adsorption of pyrene modified with carboxylic groups (PY). The decrease in roughness observed by AFM for the fG containing films may also contribute to the WCA decrease.

### *2.3.6. Water Uptake*

The WU ability of the produced multilayered FS films was evaluated by immersion in phosphate buffer solution (PBS) at 37 °C during 48 h, and the results are presented in **Figure 11**a. The control films reached the WU equilibrium after 4 h, with a maximum WU of ≈250%. The incorporation of fG in the FS multilayer films reduced the WU to a maximum of ≈230% and the equilibrium was reached after 7 h. These results are in agreement with a previous work reported for multilayered FS films based on ALG, CHI, and graphene with a different functionalization.[42] The delay observed in the equilibrium time may be due to the 2D nature and barrier properties of the fG flakes, delaying the diffusion of water through the film.[58,65] The few-layer graphene flakes are intrinsically hydrophobic, only their surface was modified to become hydrophilic, and thus the weight fraction of fG incorporated in the FS film may have little contribution to the overall WU. Also, the establishment of a good interface between CHI/fG may result in lower ability for water uptake. Thus, the addition of fG(XGC) to CHI/ALG multilayered FS films appears to be a suitable and simple strategy to control the water uptake, avoiding more complex chemical methods.

### *2.3.7. Degradation Tests*

The weight loss of control and fG FS multilayered films caused by nonenzymatic hydrolysis and enzyme-catalyzed

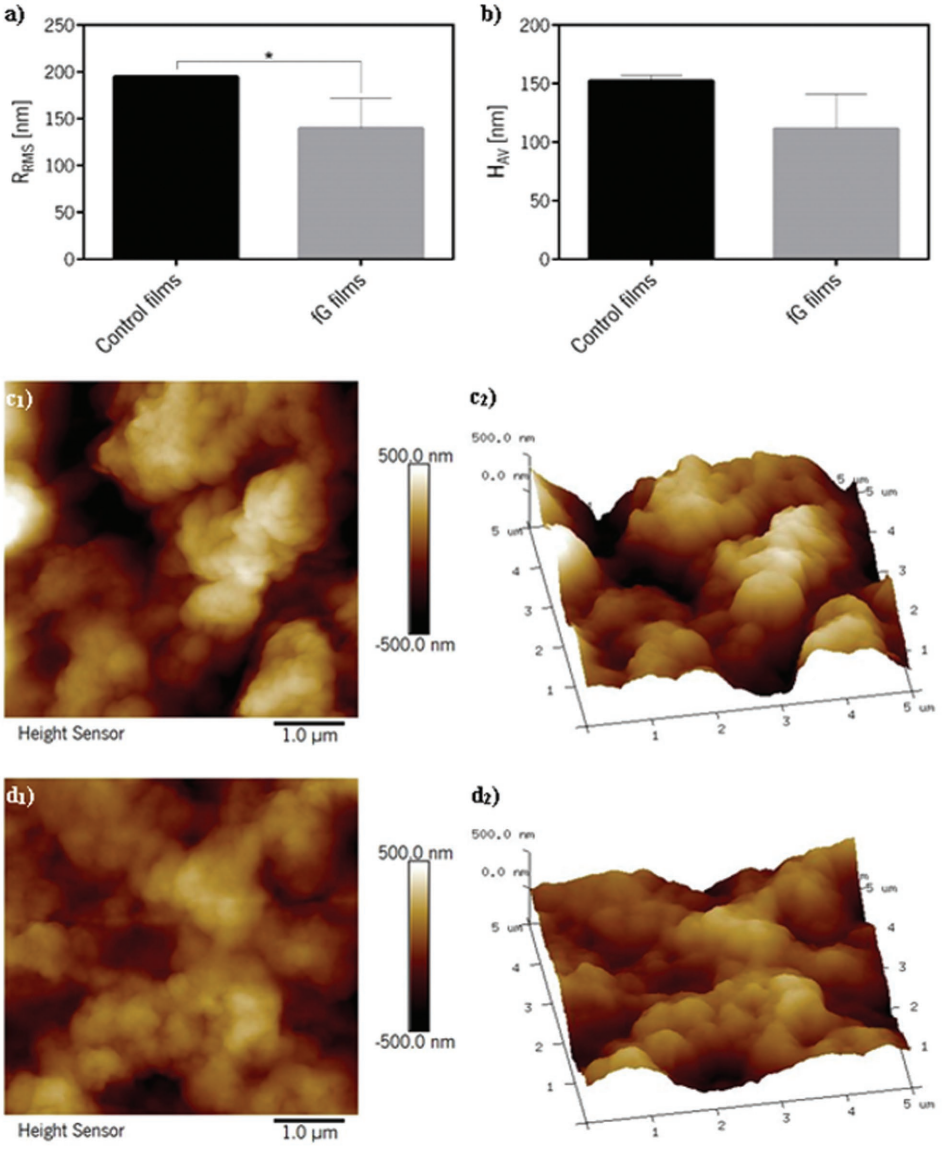


**Figure 9.** a) $R_{RMS}$ and b) $H_{AV}$. AFM surface images with respective 3D representations of $c_1$,$c_2$) control films and $d_1$,$d_2$) fG films. Significant differences were found for $p < 0.05$ (*).

hydrolysis, which represent two degradation processes commonly occurring in natural polymers,[66,67] were evaluated. Enzyme-catalyzed hydrolysis studies were carried out using lysozyme, an enzyme present in human serum in concentration between 0.004 and 0.013 mg $mL^{-1}$, typically involved in the degradation of chitin derivatives such as CHI.[67] The maximum lysozyme concentration was employed in this study. Figure 11b presents the weight loss undergone by the FS multilayered films when immersed in PBS and PBS + lysozyme during 7, 14, 21, and 28 d. After 7 d in PBS a weight loss of 21% and 13% for the control and fG films, respectively, was observed. The equivalent study using PBS + lysozyme showed a weight loss of ≈27% for the control films and 14% for fG containing films. A similar tendency was reported by Justin et al. showing an initial high degradation rate in PBS medium containing lysozyme as a consequence of the lysozyme reaction with the abundant chitosan chains containing at least three acetyl units.[68] At the end of 28 d, control FS films reached a weight loss of about 25% and 30% in PBS and PBS + lysozyme medium, respectively. Under the same conditions the weight loss measured for fG FS films was ≈16% in PBS and 17% in PBS with lysozyme. Lysozyme had a considerable effect on the degradation of the control FS films, but almost no effect on the fG containing films. Overall, the weight loss of the control FS films was always greater than observed for fG containing films. The incorporation of fG enhanced the degradation resistance of the CHI/ALG multilayered films, in agreement with previous work reported.[42] The lower WU observed for the fG containing FS multilayered films may aid to increase the stability of this film toward PBS and PBS + lysozyme degradation compared to the CHI/ALG FS film. Similar results were reported in the literature for CHI

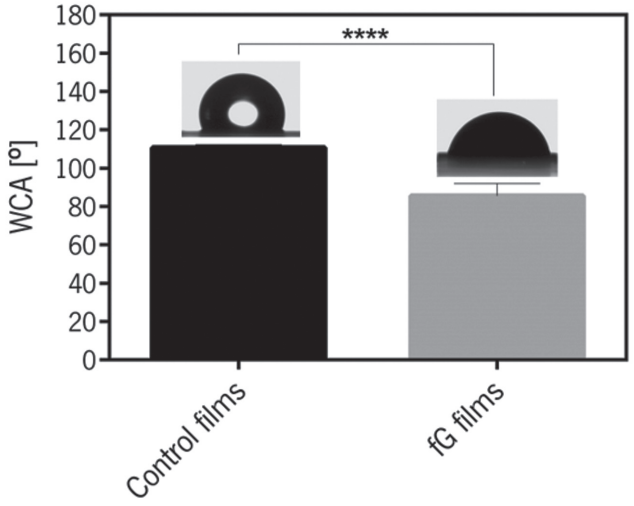


**Figure 10.** WCA results with representative images for the surface of control and fG FS films. Significant differences were found for $p < 0.0001$ (****).

composites, where a decrease in weight loss and degradation rate of CHI was observed after the incorporation of GO.[65,69]

### 2.3.8. Mechanical Characterization

The mechanical/viscoelastic properties of the control and fG FS multilayered films were evaluated by dynamical mechanical analysis (DMA). **Figure 12**a presents the variation of the storage modulus, $E'$, as a function of the frequency. Overall, it was observed that $E'$ increases with frequency, a characteristic behavior of viscoelastic materials.[63,70] The incorporation of fG(XGC) in the FS multilayered films increased the stiffness, as expected considering the much higher modulus of fG compared to CHI and ALG. Other works report a similar effect for the incorporation of graphene derivatives on CHI[71,72] and on ALG[59] to form composites, a significant increase in stiffness being observed with the addition of graphene derivatives at a concentration as low as 0.1 wt%.

Figure 12a shows that $E'$ increased by nearly 2.5 times for fG FS films relative to the control FS films, comparable to the results reported in a previous work for CHI/ALG/CHI/GO multilayered films.[42] No considerable variations were observed for the loss factor, tan $\delta$, with the increase of the frequency (Figure 12b). The incorporation of fG(XGC) in the FS multilayered films led to a decrease in tan $\delta$, from 0.6 to 0.2, approximately, in the range of frequencies analyzed. Such decrease in tan $\delta$ shows that the inclusion of fG on the FS films has a similar effect to that observed on FS films subject to crosslinking, enhancing the elastic character of the control FS films.[63,73] The tan $\delta$ results indicate that FS films with and without fG present a viscoelastic character, which is relevant to mimic living tissue for biomedical applications.[62,74] A similar behavior was observed before for FS multilayered films based on CHI, ALG, and GO.[42]

The control FS films and the films containing fG were subject to uniaxial tensile testing, yielding stress–strain curves as represented in Figure 12c. Figure 12d–f presents the ultimate tensile strength (UTS), strain at break ($\varepsilon_B$), and Young's modulus results, respectively, obtained from statistically meaningful analysis of the stress–strain curves. It was observed that UTS increased by 125% and $\varepsilon_B$ by 27% with the incorporation of fG in the FS multilayered films. According to Wan et al., the properties of the graphene derivative, its exfoliation state and the interfacial interaction with the polymer play a major role on its reinforcement effect.[75] The UTS values of the control and fG FS films are found within the typical values for aorta and skin tissue, respectively, which indicates that these materials may be adequate for the regeneration of small defects in these tissues.[76] The increase in the UTS and $\varepsilon_B$ may result from the homogeneous distribution of parallel aligned functionalized few-layer graphene over the polymeric layers and the strong interfacial adhesion between the graphene derivative and the polymeric material, as reported in previous works on composites based on CHI and graphene derivatives,[72,77] and on multilayered FS films based on CHI, ALG, and GO.[42] The simultaneous improvement in the mechanical strength and ductility of polymer nanocomposites has been reported with the incorporation of other oriented or functionalized carbon nanofillers, such as carbon nanotubes.[78,79] The Young's modulus of the FS multilayered films also increased with the incorporation of fG(XGC) as observed in Figure 12f. A similar behavior was observed in previous works where the incorporation of graphene derivatives on ALG[58] and CHI[72,80] films led to an increase in their Young's modulus.

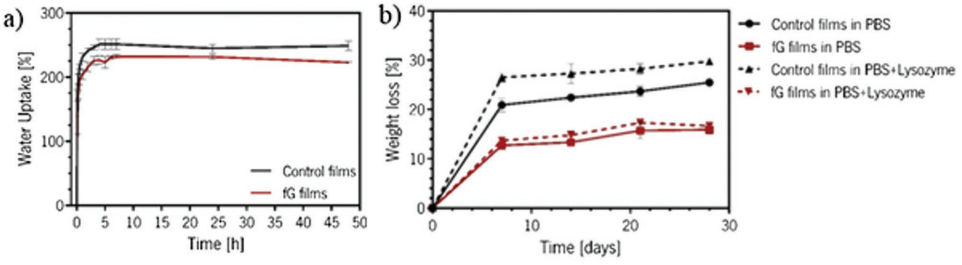


**Figure 11.** a) Variation of the WU ability as a function of time for control and fG FS films in PBS at 37 °C and b) degradation behavior measured as weight loss of control and fG FS films immersed in PBS or PBS with lysozyme over a period of 28 d at 37 °C.

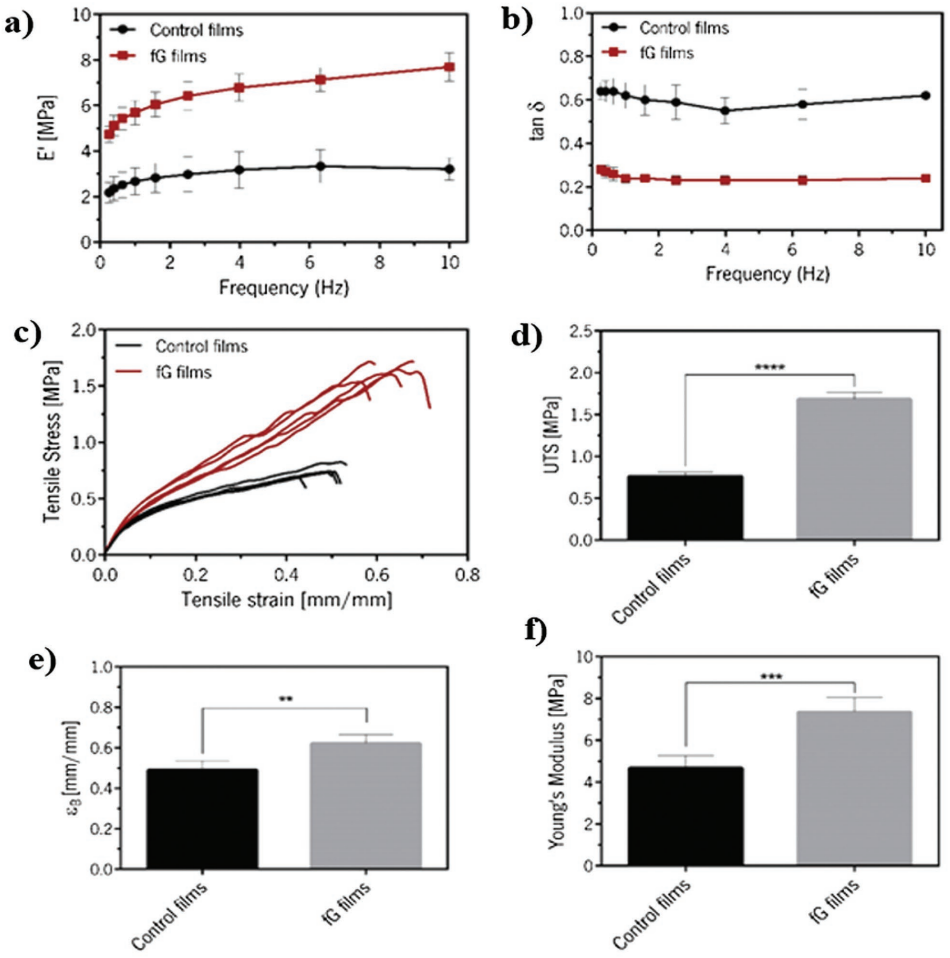


**Figure 12.** DMA results for the FS multilayered films immersed in PBS, at 37 °C, to simulate the physiological conditions: variation of the storage modulus a) and loss factor b) along a frequency scan ranging from 0.2 to 10 Hz; stress–strain curves obtained from tensile tests c), and results obtained for UTS d), breaking strain e) and Young's modulus f). Significant differences were found for $p < 0.0001$ (****), $p < 0.001$ (***), and $p < 0.01$ (**).

### *2.3.9. Electrical Properties*

The electrical resistivity of the FS multilayered films was measured by measuring the current intensity versus voltage (*I*–*V*) curves in the voltage range from −5 to 5 V, as depicted in **Figure 13**. The electrical resistivity was computed considering the current passing through the sample in the voltage range between −1.0 and 1.0 V (inset in Figure 13). The incorporation of fG(XGC) in the multilayered FS films resulted in a decrease of the electrical resistivity from $3.0 \times 10^{12}$ to $5.3 \times 10^{10}$ Ω m. Several works report considerably lower electrical resistivity for composites containing graphene derivatives as fillers, even at contents as low as 1.0 wt%.[56,69,81–83] However, in order to reach electrical percolation a higher content of the graphene derivative is typically required. Li et al. reported a similar electrical resistivity for GO/polystyrene composites (1.0 wt% in GO) to that obtained in the present work.[84] The polyelectrolyte sequence used for the production of the multilayered FS films may significantly influence their electrical properties. In fact, the deposition of three polymer layers followed by one graphene layer may limit the volume conductivity measured through the cross-sectional direction. However, although the FS multilayered films remain resistive after the incorporation of fG(XGC), their resistivity decreased by two orders of magnitude, which is a good indicator for the possibility of producing conductive films at higher graphene content.

### *2.3.10. Biological Studies*

L929 fibroblasts cells were used to evaluate the in vitro cytocompatibility of the produced multilayered FS films during 1, 3, and 7 d. 4′,6-Diami-dino-2-phenylindole (DAPI)-phalloidin test (**Figure 14**) was performed to understand how L929 cells adhered and which morphology they presented on the surface of the produced FS films. At day 1, the cells presented a round shape typical of the short culture period and started to adhere on the surface of the produced multilayered FS films. Some aggregates of cells were found mainly for the control FS films. After a period of 3 and 7 d of culture, the L929 cells presented a spread morphology and an increase in

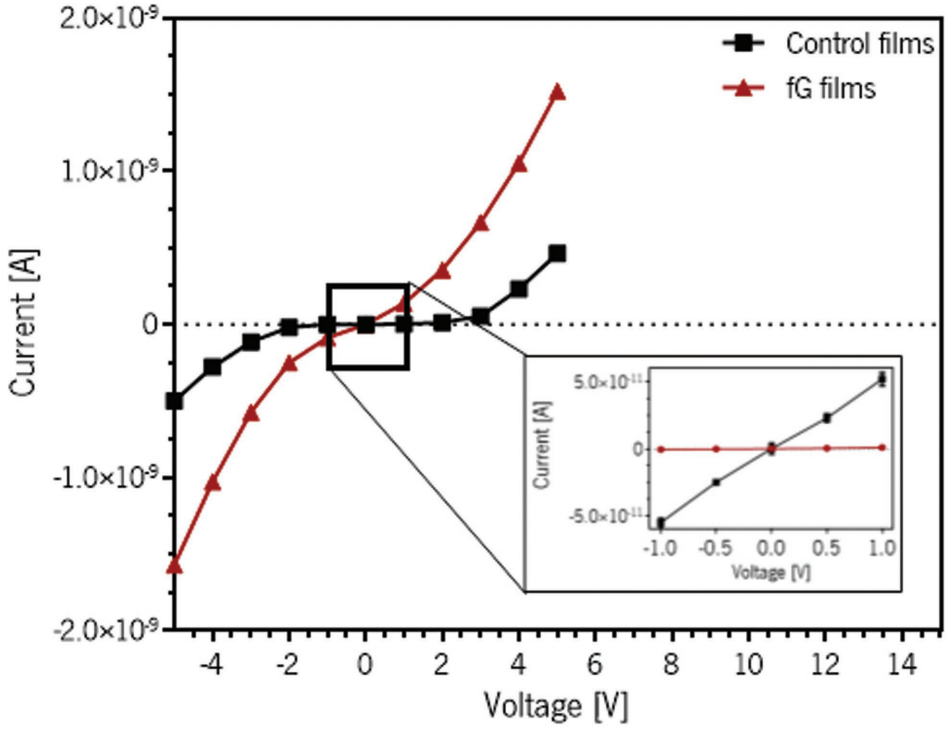


**Figure 13.** *I–V* curves of the control and fG films between with inset showing in detail the region between −1.0 and 1.0 V.

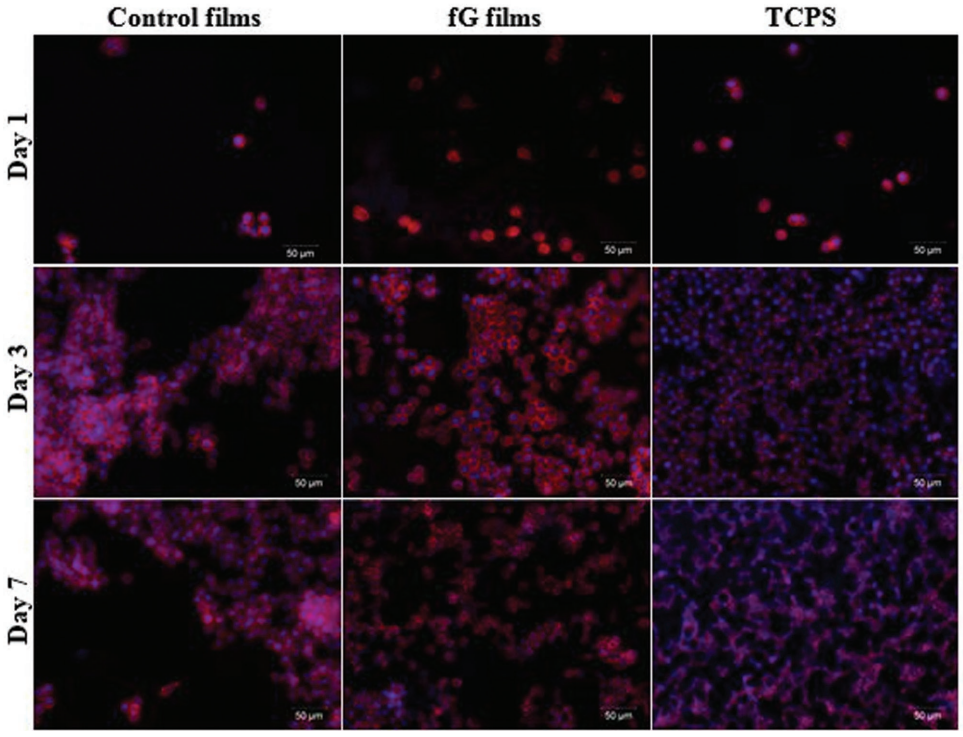


**Figure 14.** Representative photographs of cells' morphology using DAPI for nuclei staining (blue labeled) and phalloidin for F-actin filaments staining (red labeled) by fluorescence microscopy at 1, 3, and 7 d post-seeding on control films, fG films, and TCPS.

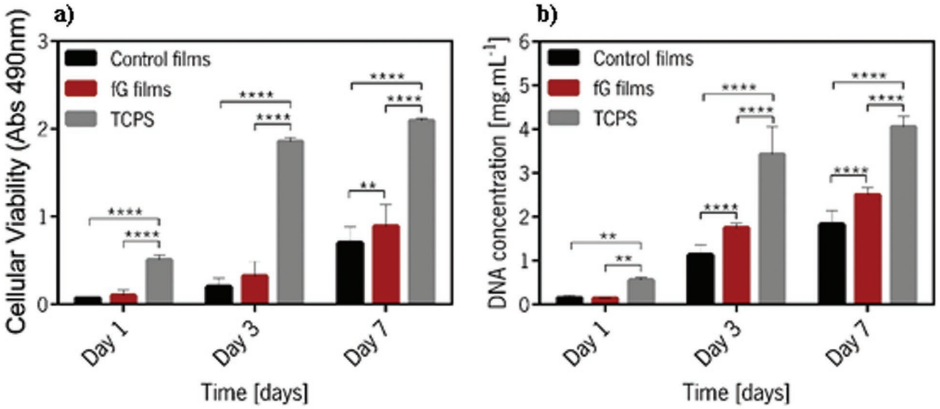


**Figure 15.** a) Metabolic activity analysis for control and fG FS multilayered films using MTS assay for 1, 3, and 7 d. b) DNA quantification assay performed on control and fG films. Significant differences were found for $p < 0.0001$ (****) and $p < 0.01$ (**).

cell number was noticed. Such increase in cell proliferation was even more pronounced at day 7 where almost all the surface area of the multilayered FS films was covered by adhered cells, especially for the fG FS films. Moreover, the produced multilayered FS films revealed a similar morphology and behavior when compared with tissue culture polystyrene (TCPS).

The metabolic activity on the produced FS multilayered films was evaluated by the 3-(4,5-dimethylthiazol-2-yl)-5-(3 carboxymethoxyphenyl)-2-(4-sulphophenyl)-2H-tetrazolium (MTS) colorimetric assays and the results are presented in **Figure 15**a. The metabolic activity increased with increasing culturing time, suggesting good cell viability on the surfaces of the multilayered FS films. Overall, TCPS present significant differences in relation to both control and fG FS films ($p < 0.0001$). On day 7, significant differences were observed between control FS films and fG FS films ($p < 0.01$). Such results revealed that the produced multilayered FS films containing fG(XGC) allowed L929 cells to express better metabolic activity. Similar results have been reported in the work of Moura et al. where an improvement of the metabolic activity was verified when the GO in the form of flakes were included in FS multilayered films with CHI and ALG as matrix.[42] The cell proliferation over a period of 7 d was assessed by DNA quantification (Figure 15b). Overall, an increase in cell proliferation was verified for all formulations. Comparing all the formulations with TCPS at day 1, significant differences were observed for both control and fG FS films ($p < 0.01$). At days 3 and 7 significant differences were also found between the TCPS and both control and fG FS films ($p < 0.0001$). Moreover, at these time points significant differences were observed between control FS films and fG FS films ($p < 0.0001$).

Taken altogether, the preliminary biological assays indicate that the presence of fG(XGC) on the multilayered FS films lead to an increase on the metabolic activity and cell proliferation of L929 cells. The enhancement on cells' spreading and proliferation might be related with the hydrophilic behavior of fG FS films against the hydrophobic character of control FS films. According with the literature, cells' adhesion to moderate hydrophilic surfaces is favored in comparison with hydrophobic or super hydrophilic surfaces.[85] Furthermore, the increasing in stiffness along with the decreasing in WU ability might also have contributed to an improved cellular behavior, once cells appear to prefer stiffer and lower hydration multilayered films.[86,87] The results obtained in this work are similar to other works where the biological performance of graphene-based composites was evaluated.[65,71] Thus, since a significant increase of the cell proliferation was observed as well as an increase of the FS films stiffness and thermal stability, these multilayered films may find a wide number of applications, such as wound healing, cardiac and bone engineering.

## 3. Conclusions

A simple method was adopted in this work for the noncovalent functionalization of graphite and preparation of few-layer graphene. fG FS multilayered films with CHI and ALG were successfully produced through LbL assembly. The addition of few-layer graphene induced significant changes in the properties of the produced FS films. TGA analysis revealed an overall weight content of fG(XGC) of ≈1%, uniformly distributed along the FS film, as demonstrated by Raman mapping. It was found that the incorporation of fG(XGC) did not change the morphology of the film surface at the microscale, when compared with the control films. Moreover, the FS films containing fG(XGC) revealed an enhancement of the UTS, strain at break and Young's modulus. A decrease in the nanoroughness of these FS films was also verified as well as a change from a hydrophobic to a hydrophilic behavior. The resistance to degradation was enhanced while the water absorption ability of the FS films decreased with the presence of fG(XGC). Such films also showed a two order of magnitude decrease in electrical resistivity. The preliminary biological assays revealed that L929 cells were viable and able to proliferate over a period of 7 d on the developed fG FS films. Finally, according to the results obtained, it was demonstrated that the $(CHI/ALG/CHI/fG(XGC))_{100}$ FS multilayered films exhibit interesting properties which can be essential for biomedical applications such as wound healing, and tissue engineering of cardiac and bone tissues.

## 4. Experimental Section

### 4.1. Materials

Three different types of graphite were used in the production of functionalized few-layer graphene aqueous suspensions. Micrograf HC11, an EG with 99.5% purity and median particle diameter ($d_{50}$) of 11 µm was obtained from Nacional de Graphite Ltda. (Brazil). Natural graphite Graphexel was obtained from Graphexel Ltd. (United Kingdom). Graphite nanoplatelets, xGnP Grade C, with bulk density within 0.2–0.4 g $cm^{-3}$ and particle diameter lower than 2 µm was purchased from XG Sciences (USA). These graphite products will be designated in this work by Micrograf (pristine), Graphexel (pristine), and XGC (pristine), respectively.

For the QCM-D studies and the production of the FS multilayered films, CHI (medium molecular weight) with deacetylation degree between 75% and 85% and viscosity ranging from 0.2 to 0.8 Pa $s^{-1}$ was purchased from Sigma-Aldrich. Before using, CHI was purified through a recrystallization process. ALG from brown algae with viscosity between 0.005 and 0.040 Pa $s^{-1}$ was purchased from Sigma-Aldrich and used as received.

### 4.2. Preparation of PY/Graphite Suspensions

PY/graphite suspensions were prepared by adding 7.9 mg to 500 mL of distilled water (DW) to produce $5 \times 10^{-5}$ M solution. The pH of this solution was adjusted to 7 to aid the total dissolution of the pyrene derivative, assisted by sonication. Then, 500 mg of graphite was added to the PY solution, and the suspension, with approximate concentration of 1 mg $mL^{-1}$, was exposed to sonication during 4 h. After sonication, the functionalized few-layer graphene suspension was centrifuged at 3500 rpm during 30 min, to remove the larger aggregates of nonexfoliated graphite, and the supernatant was collected and kept to be characterized and used in QCM-D and LbL experiments.

### 4.3. Characterization of Functionalized Few-Layer Graphene

Raman Spectroscopy analysis was performed on a LabRAM HR Evolution Raman spectrometer (Horiba Scientific, Japan) using a laser excitation wavelength of 532 nm. The functionalized few-layer graphene aqueous suspensions prepared were sprayed on a glass slide positioned on a heating plate for fast water evaporation and deposition of the graphene products to be analyzed. UV–vis Spectroscopy analysis was performed in order to determine the concentration of the functionalized few-layer graphene aqueous suspensions, using a UV-2401 PC spectrophotometer (Shimadzu, Japan) with 1 cm path length quartz cells. For the UV–vis measurements, the fG(XGC) suspension was diluted 25 times before the analysis since the as prepared suspension was too concentrated for the application of the Lambert–Beer equation. The evaluation of the thermal stability of the functionalized few layer graphene products was performed by TGA analysis using a Q500 equipment (TA Instruments, USA). The analysis was performed under a nitrogen atmosphere in the temperature range from 40 to 845 °C and scanning rate of 10 °C $min^{-1}$. The stability of the functionalized few-layer graphene suspensions was evaluated using a Zetasizer Nano-Zs equipment (Malvern Instruments, UK). The results presented are the average of at least five ZP measurements performed for each suspension.

### 4.4. Real-Time Monitoring of the Multilayered Films' Production

CHI (Polycation), ALG (Polyanion), and fG(XGC) (Polyanion) were combined to form a multilayered film with four tetralayers. The sequence of deposition used was $(CHI/ALG/CHI/fG(XGC))_4$. Adsorption took place at 25 °C, using solutions at 0.5 mg $mL^{-1}$ and at a constant flow rate of 50 mL $min^{-1}$, with an adsorption time of 10 min (starting with CHI) and an intermediate rinsing step of 5 min. The fG(XGC) suspension used in this experiment had pH 7.5. All QCM-D experiments were performed in a QCM-D E4 (Q-Sense Instruments, Sweden) and CHI and ALG solutions were freshly prepared at a concentration of 0.5 mg $mL^{-1}$ and the pH of the solutions was adjusted to pH 5.5. The data from QCM-D experiments were modeled with the Qtools software (Q-sense AB). After providing the values of $\rho_B$, $\eta_B$, and $\rho_L$, the software performs the modeling of the experimental data according to a Voigt-based model, using three overtones of frequency and dissipation. The thickness, viscosity, and shear modulus of the produced films were estimated by this model.

### 4.5. Production of the FS Multilayered Films

The multilayered FS films were produced by the LbL technique using a homemade dipping robot. Two types of multilayered FS films with different compositions were produced, $(CHI/ALG/CHI/ALG)_{100}$ as control and $(CHI/ALG/CHI/fG(XGC))_{100}$, both with 100 tetralayers. Before films buildup, polypropylene substrates were rinsed with ethanol and DW and dried with compressed air. CHI and ALG solutions were freshly prepared at a concentration of 2 mg $mL^{-1}$ and the pH of the solutions was adjusted to 5.5. The functionalized few-layer graphene suspension used to produce $(CHI/ALG/CHI/fG(XGC))_{100}$ films had a concentration of 0.25 mg $mL^{-1}$ and a pH of ≈7.5. The substrate was immersed sequentially in CHI and ALG and fG solutions during 6 min for each solution and intermediate rinsing step, with DW during 4 min, was performed between the deposition of each PE and fG depositions. After 100 cycles of deposition, the multilayered FS films were let to dry at room temperature and were easily detached from the underlying substrate, just by peeling off with the help of a tweezer. $(CHI/ALG/CHI/ALG)_{100}$ and $(CHI/ALG/CHI/fG(XGC))_{100}$ are referred in this work as control FS films and fG FS films, respectively.

### 4.6. Characterization of the FS Multilayered Films

Raman spectroscopy analysis was performed on a LabRAM HR Evolution Raman Spectrometer (Horiba Scientific, Japan) under a laser excitation wavelength of 532 nm, to assess the presence of fG(XGC) in the multilayered FS films and map the distribution of the graphene-based products across the films. The analysis was carried out on the multilayered FS films that were placed on a glass coverslip. The spectra were recorded at RT and the results were analyzed using the LabSpec6 software.

TGA analysis was performed to estimate the amount of fG products incorporated in the multilayered FS films and to evaluate the thermal stability of both fG and control FS films. TGA was carried out on a Q500 equipment (TA Instruments, USA) under nitrogen atmosphere, within a temperature range from 40 to 845 °C and scanning rate of 10 °C $min^{-1}$.

The weight content of few-layer graphene in the LbL films was estimated considering the TGA weight losses observed at 840 °C for CHI/ALG (control films), fG-multilayered films, and also considering the weight loss of as-produced fG.

The morphology of the multilayered FS films was characterized using a JSM-6010LV SEM (JEOL, Japan) microscope, operating at 15 kV. Before the analyses, the samples were coated with a gold layer, using an EM ACE600 (Leica Microsystems, Germany) sputter coater. For cross-sectional observations, the FS films were dipped in liquid nitrogen until free fracture.

The topography and roughness analysis was performed using a Dimension Icon AFM (Bruker, France) with an air cantilever (SNL-10D) (Bruker, France) with a spring constant of 0.06 N $m^{-1}$, operating in a ScanAsyst mode. The topography of the multilayered FS films was investigated with $512 \times 512$ pixels$^2$ at line rates of 1 Hz. For surface roughness analysis, AFM images with $5 \times 5$ µm$^2$ were obtained, followed by root mean squared roughness ($R_{RMS}$) and average height ($H_{av}$) values calculation. At least three measurements were carried out for both

control and fG FS films. The analysis of the images was performed using the software NanoScope Analysis.

The wettability of the multilayered FS films was evaluated by WCA measurements using an OCA15plus goniometer equipment (DataPhysics, Germany). At least five measurements were performed, at RT, by dispensing drops of 5 µL of DW. The pictures were acquired as the drop contacted the surface of the FS films and the results were treated using the SCA20 software.

Water uptake (WU) experiments were performed to evaluate the swelling ability of the produced multilayered FS films. The WU values were obtained by weighing the samples, from both control and fG FS films, before and after immersion in PBS solution at 37 °C for 5, 15, and 30 min, and 1, 2, 3, 4, 5, 6, 7, 24, and 48 h. At each time point, the samples were taken from the medium and the excess of solution was removed with a filter paper, before weighing. Finally, the WU was calculated using Equation (1)

$$\text{Water uptake}\,(\%) = \frac{m_w - m_i}{m_i} \times 100 \quad (1)$$

where $m_i$ is the initial dry mass of a sample before immersion and $m_w$ is the mass of the swelled sample at a given time point.

The weight loss of both multilayered films caused by nonenzymatic hydrolysis and enzyme-catalyzed hydrolysis, which represent two degradation processes commonly occurring in polymers of natural origin, was evaluated through degradation tests. The weight loss of the multilayered FS films was determined by weighing the samples before and after immersion in PBS solution with sodium azide (0.02% w/v) as well as in PBS solution with lysozyme in a concentration of 0.013 mg $mL^{-1}$, at 37 °C, for 7, 14, 21, and 28 d. At each time point, the samples were removed from the solution, washed with distilled water, and dried and, subsequently weighed. The weight loss was calculated using Equation (2)

$$\text{Weight loss}\,(\%) = \frac{m_i - m_f}{m_i} \times 100 \quad (2)$$

where $m_i$ is the initial dry mass of a sample before immersion and $m_f$ is the mass of the dried sample at a given time point.

The tensile properties of the multilayered FS films were evaluated through Uniaxial Tensile Tests, following ASTM D3039/D3039M-14, in a Universal Mechanical Testing machine (Instron 5543, USA) equipped with a 1 kN load cell. The specimens were cut with rectangular shape, with ≈5 mm width, and were subjected to a strain rate of 1 mm $min^{-1}$ at a gauge length of 10 mm. At least five samples, from both fG and control FS films, were tested, after immersion overnight in a PBS solution. The cross-sectional area of the FS films was measured immediately before the tests, where the thickness was determined in three different regions of each sample using a micrometer (Mitutoyo, Japan). Finally, the ultimate tensile strength, elongation at break, and Young's modulus of the multilayered FS films were calculated, according to the standard indicated.

The mechanical/viscoelastic properties of the multilayered FS films were evaluated using DMA. The DMA experiments were performed using a Tritec2000B DMA (Triton Technology (UK)), equipped with the tensile mode. The multilayered FS films were cut with ≈5 mm width. Prior to the DMA assays, the samples were soaked overnight in a PBS solution, to reach the swelling equilibrium. The geometry of the samples was then measured accurately for each sample, where the thickness was determined in three different regions using a micrometer (Mitutoyo, Japan). The measurements were carried out at 37 °C with the multilayered FS films immersed in a PBS solution placed in a Teflon reservoir. The multilayered FS films were clamped in the DMA apparatus with a gauge length of 10 mm and immersed in the PBS bath. After stabilizing at 37 °C, the DMA spectra were obtained during a frequency scan between 0.2 and 10 Hz. The experiments were performed under constant strain amplitude (50 µm) and a static preload of 1 N was applied during the tests to keep the sample tight. At least three specimens were tested for each condition with the same experimental settings.

The electrical conductivity measurements were performed following ASTM D257, using with a picoammeter 6487 (Keithley, USA) with 8009 electrodes (Keithley, USA). Direct current measurements were performed for voltages varying between −5.0 and 5.0 V. The samples were rectangular with an area of $1.68 \times 10^{-4}$ $m^2$. The thickness of the samples was measured before the tests using a micrometer (Mitutoyo, Japan). The results presented are the average of 100 measurements performed for each voltage applied.

L929 mouse fibroblasts line (L929, European Collection of Cell Cultures) was used to test the in vitro biocompatibility of the control and fG multilayered FS films for 1, 3, and 7 d. Cells were cultured in complete Dulbecco's modified minimum essential medium (DMEM) medium supplemented with 3.7 g $L^{-1}$ sodium bicarbonate, 10% fetal bovine serum, and 1% penicillin-streptomycin (pH = 7.4), in 150 $cm^2$ tissue culture flasks and incubated at 37 °C in a humidified air atmosphere of 5% $CO_2$. The medium was replaced every 2–3 d.

Prior to cell seeding, samples with $10 \times 10$ $mm^2$ were sterilized by immersion in 70 vol% ethanol for 2 h and then washed twice with sterile PBS. After this, the multilayered FS films were immersed in cell culture medium for complete swelling. The cells were seeded in the multilayered FS films at a density of 50 000 cells per sample and nourished with DMEM. The cultures were incubated at 37 °C in a humidified air atmosphere of 5% $CO_2$.

The morphology and viability of the cells was assessed using fluorescence staining with phalloidin tetramethylrhodamine and DAPI. At each time point DAPI (20 mg $mL^{-1}$, Sigma-Aldrich) and phalloidin (20 mg $mL^{-1}$, Sigma-Aldrich) were used. Prior to staining, culture medium was removed and the multilayered FS films were washed with sterile PBS. Formalin (10%, ThermoFisher) was added for 30 min, to fix the cells of the above samples. After that, formalin was removed and the samples were washed with PBS. Following this, 1 mL of PBS with 10 µL of phalloidin was added and kept at RT, protected from light, during 45 min. Subsequently, the samples were washed with PBS and stained with 1 µL of DAPI in 1 mL of PBS for 15 min. After 15 min, the samples were washed again with PBS and images were obtained using an inverted fluorescence microscope (Zeiss, Germany).

The metabolic activity of the L929 cells was measured using the 3-(4,5-dimethylthiazol-2-yl)-5-(3-carboxymethoxyphenyl)-2-(4-sulphophenyl)-2H-tetrazolium (MTS colorimetric assay, Cell Titer 96 AQueous One Solution Cell Proliferation Assay, Promega, USA). At each time point the samples were washed with PBS and then immersed in an MTS solution, prepared by using a 1:5 ratio of MTS reagent and serum free cell culture medium and let to incubate in this solution for 3 h at 37 °C with a humidified atmosphere containing 5% $CO_2$ in the dark. Afterward, 0.1 mL (in triplicate) of each well were transferred to a new 96-well plate and finally the optical density was read at 490 nm on a multiwell microplate reader (Synergy HT, Bio-Tek Instruments). At least four samples, from both control and fG FS films, were tested.

Cell proliferation into the developed FS multilayered films was also investigated through the quantification of double-stranded DNA (dsDNA) for 1, 3, and 7 d. First, cells were lysed by osmotic and thermal shock and the obtained supernatant was analyzed using PicoGreen dsDNA kit (Life Technologies, UK). The recovered supernatant was read on a microplate reader (BioTek, USA) using a 485 and 528 nm as excitation and emission wavelengths, respectively. Triplicates were performed for each sample and the DNA amounts were calculated using a standard curve.

### 4.7. Statistical Analysis

Data were expressed as average ± standard deviation (SD) of at least three replicates. The error bars present in the graphics denote the SD. Normality tests were performed using D'Agostino and Pearson test. For the uniaxial tensile tests, AFM assays, and WCA assays the population was normally distributed and unpaired parametric *t*-test were used. For biological assays, Two-Way Anova, followed by Turkey's test, was used. The statistical analysis was performed using the software GraphPad

Prism 6.0 for Windows. Statistical significance was accepted for a $p < 0.05$ (*).

## Acknowledgements

The authors acknowledge the Portuguese Foundation for Science and Technology (FCT) and the European program FEDER/COMPETE for the financial support through projects UID/Multi/50026/2013 and UID/CTM/50025/2013. This work was also financially supported by FCT through the scholarships SFRH/BPD/96797/2013 granted to Sofia G. Caridade, SFRH/BD/97606/2013 granted to Maria P. Sousa, and SFRH/BD/87214/2012 granted to Eunice Cunha.

## Conflict of Interest

The authors declare no conflict of interest.

## Keywords

biomedical applications, freestanding multilayered films, functionalized graphene, natural polymers

Received: June 28, 2017
Revised: December 18, 2017
Published online:

[1] M. Terrones, A. R. Botello-Méndez, J. Campos-Delgado, F. López-Urías, Y. I. Vega-Cantú, F. J. Rodríguez-Macías, A. L. Elías, E. Muñoz-Sandoval, A. G. Cano-Márquez, J. C. Charlier, H. Terrones, *Nano Today* **2010**, *5*, 351.
[2] A. H. Castro Neto, F. Guinea, N. M. R. Peres, K. S. Novoselov, A. K. Geim, *Rev. Mod. Phys.* **2009**, *81*, 109.
[3] H. O. Pierson, *Handbook of Carbon, Graphite, Diamond and Fullerenes*, Noyes Publication, Park Ridge, NJ **1994**.
[4] K. S. Novoselov, V. I. Fal'ko, L. Colombo, P. R. Gellert, M. G. Schwab, K. Kim, *Nature* **2012**, *490*, 192.
[5] X. Huang, X. Qi, F. Boey, H. Zhang, *Chem. Soc. Rev.* **2012**, *41*, 666.
[6] C. Lee, X. Wei, Q. Li, R. Carpick, J. W. Kysar, J. Hone, *Phys. Status Solidi B* **2009**, *246*, 2562.
[7] Y. Zhu, S. Murali, W. Cai, X. Li, J. W. Suk, J. R. Potts, R. S. Ruoff, *Adv. Mater.* **2010**, *22*, 3906.
[8] M. Pumera, *Chem. Rec.* **2009**, *9*, 211.
[9] D. Li, M. B. Müller, S. Gilje, R. B. Kaner, G. G. Wallace, *Nat. Nanotechnol.* **2008**, *3*, 101.
[10] N. Pu, C. Wang, Y. Liu, Y. Sung, D. Wang, M. Ger, *J. Taiwan Inst. Chem. Eng.* **2012**, *43*, 140.
[11] J. Liu, J. Tang, J. J. Gooding, *J. Mater. Chem.* **2012**, *22*, 12435.
[12] X. Qi, K. Pu, H. Li, X. Zhou, S. Q. Fan, B. Liu, F. Boey, W. Huang, H. Zhang, *Angew. Chem., Int. Ed.* **2010**, *49*, 9426.
[13] D. Parviz, S. Das, H. S. T. Ahmed, F. Irin, S. Bhattacharia, M. J. Green, *ACS Nano* **2012**, *6*, 8857.
[14] L. Li, X. Zheng, J. Wang, Q. Sun, Q. Xu, *ACS Sustainable Chem. Eng.* **2013**, *1*, 144.
[15] A. Sionkowska, *Prog. Polym. Sci.* **2011**, *36*, 1254.
[16] a) K. Y. Lee, D. J. Mooney, *Prog. Polym. Sci.* **2012**, *37*, 106; b) H. R. Allcock, *Introduction to Materials Chemistry*, Wiley, Hoboken, NJ **2008**.
[17] E. P. Ivanova, K. Bazaka, R. J. Crawford, *New Functional Biomaterials for Medicine and Healthcare*, Woodhead Publishing, Oxford, UK **2013**.
[18] M. Vakili, M. Rafatullah, B. Salamatinia, A. Z. Abdullah, M. H. Ibrahim, K. B. Tan, Z. Gholami, P. Amouzgar, *Carbohydr. Polym.* **2014**, *113*, 115.
[19] M. Rinaudo, *Prog. Polym. Sci.* **2006**, *31*, 603.
[20] C. Pandis, S. Madeira, J. Mato, A. Kyritsis, J. F. Mano, J. L. G. Ribelles, *Mater. Sci. Eng., C* **2014**, *42*, 553.
[21] P. K. Dutta, J. Dutta, V. S. Tripathi, *J. Sci. Ind. Res.* **2004**, *63*, 20.
[22] I. Armentano, M. Dottori, E. Fortunati, S. Mattioli, J. M. Kenny, *Polym. Degrad. Stab.* **2010**, *95*, 2126.
[23] A. M. Pinto, I. C. Gonçalves, F. D. Magalhães, *Colloids Surf., B* **2013**, *111*, 188.
[24] K. Chen, Y. Ling, C. Cao, X. Li, X. Chen, X. Wang, *Mater. Sci. Eng., C* **2016**, *69*, 1222.
[25] W. Ye, X. Li, H. Zhu, X. Wang, S. Wang, H. Wang, R. Sun, *Chem. Eng. J.* **2016**, *299*, 45.
[26] X. Li, Y. Han, Y. Ling, X. Wang, R. Sun, *ACS Sustainable Chem. Eng.* **2015**, *3*, 1846.
[27] J. Borges, J. F. Mano, *Chem. Rev.* **2014**, *114*, 8883.
[28] A. Quinn, G. K. Such, J. F. Quinn, F. Caruso, *Adv. Funct. Mater.* **2008**, *18*, 17.
[29] Z. Tang, Y. Wang, P. Podsiadlo, N. A. Kotov, *Adv. Mater.* **2006**, *18*, 3203.
[30] K. Ariga, J. P. Hill, Q. Ji, *Phys. Chem. Chem. Phys.* **2007**, *9*, 2319.
[31] J. Cong, Y. Chen, J. Luo, X. Liu, *J. Solid State Chem.* **2014**, *218*, 171.
[32] K. Sheng, H. Bai, Y. Sun, C. Li, G. Shi, *Polymer* **2011**, *52*, 5567.
[33] S. Liu, J. Ou, Z. Li, S. Yang, J. Wang, *Appl. Surf. Sci.* **2012**, *258*, 2231.
[34] Y. Zhu, J. Ji, J. Ren, C. Yao, L. Ge, *Colloids Surf., A* **2014**, *455*, 92.
[35] J. Ma, P. Cai, W. Qi, D. Kong, H. Wang, *Colloids Surf., A* **2013**, *426*, 6.
[36] C. Shan, L. Wang, D. Han, F. Li, Q. Zhang, X. Zhang, L. Niu, *Thin Solid Films* **2013**, *534*, 572.
[37] L. Zho, D. Yang, W. Yu, J. Zhang, C. Li, *Org. Electron.* **2015**, *23*, 110.
[38] D. Zhang, J. Tong, B. Xia, *Sens. Actuators, B* **2014**, *197*, 66.
[39] X. Xu, D. Huang, K. Cao, M. Wang, S. M. Zakeeruddin, M. Grätzel, *Sci. Rep.* **2013**, *3*, 1489.
[40] L. Tang, X. Li, D. Du, C. He, *Prog. Nat. Sci.* **2012**, *22*, 341.
[41] X. Wen, Q. Cao, L. Liang, J. Chen, C. You, Y. Ruan, H. Lin, L. Wu, *Talanta* **2013**, *117*, 359.
[42] D. Moura, S. G. Caridade, M. P. Sousa, E. Cunha, H. C. Rocha, J. F. Mano, M. C. Paiva, N. M. Alves, *J. Mater. Chem. B* **2016**, *4*, 7718.
[43] L. M. Malard, M. A. Pimenta, G. Dresselhaus, M. S. Dresselhaus, *Phys. Rep.* **2009**, *473*, 51.
[44] A. C. Ferrari, *Solid State Commun.* **2007**, *143*, 47.
[45] A. C. Ferrari, D. M. Basko, *Nat. Nanotechnol.* **2013**, *8*, 235.
[46] A. C. Ferrari, J. C. Meyer, V. Scardaci, C. Casiraghi, M. Lazzeri, F. Mauri, S. Piscanec, D. Jiang, K. S. Novoselov, S. Roth, A. K. Geim, *Phys. Rev. Lett.* **2006**, *97*, 187401.
[47] Y. Y. Wang, Z. H. Ni, T. Yu, Z. X. Shen, H. M. Wang, Y. H. Wu, W. Chen, A. T. S. Wee, *J. Phys. Chem. C* **2008**, *112*, 10637.
[48] H. Shinohara, Y. Yamakita, K. Ohno, *J. Mol. Struct.* **1998**, *442*, 221.
[49] A. Viinikanoja, J. Kauppila, P. Damlin, E. Mäkilä, J. Leiro, T. Ääritalo, J. Lukkari, *Carbon* **2014**, *68*, 195.
[50] H. Yang, Y. Hernandez, A. Schlierf, A. Felten, A. Eckmann, S. Johal, P. Louette, J.-J. Pireaux, X. Feng, K. Mullen, V. Palermo, C. Casiraghi, *Carbon* **2013**, *53*, 357.
[51] J. I. Paredes, S. Villar-Rodil, A. Martínez-Alonso, J. M. D. Tascón, *Langmuir* **2008**, *24*, 10560.
[52] B. Konkena, S. Vasudevan, *J. Phys. Chem. Lett.* **2012**, *3*, 867.
[53] N. M. Alves, C. Picart, J. F. Mano, *Macromol. Biosci.* **2009**, *9*, 776.
[54] F. Höök, B. Kasemo, T. Nylander, C. Fant, K. Sott, H. Elwing, *Anal. Chem.* **2001**, *73*, 5796.
[55] S. M. Notley, M. Eriksson, L. Wågberg, *J. Colloid Interface Sci.* **2005**, *292*, 29.

[56] X. Wang, H. Bai, Z. Yao, A. Liu, G. Shi, *J. Mater. Chem.* **2010**, *20*, 9032.
[57] L. He, H. Wang, G. Xia, J. Sun, R. Song, *Appl. Surf. Sci.* **2014**, *314*, 510.
[58] M. Ionita, M. A. Pandele, H. Iovu, *Carbohydr. Polym.* **2013**, *94*, 339.
[59] L. Nie, C. Liu, J. Wang, Y. Shuai, X. Cui, L. Liu, *Carbohydr. Polym.* **2015**, *117*, 616.
[60] S. G. Caridade, C. Monge, F. Gilde, T. Boudou, J. F. Mano, C. Picart, *Biomacromolecules* **2013**, *14*, 1653.
[61] J. M. Silva, S. G. Caridade, N. M. Oliveira, R. L. Reis, J. F. Mano, *J. Mater. Chem. B* **2015**, *3*, 4555.
[62] J. M. Silva, A. R. C. Duarte, S. G. Caridade, C. Picart, R. L. Reis, J. F. Mano, *Biomacromolecules* **2014**, *15*, 3817.
[63] S. G. Caridade, C. Monge, J. Almodóvar, R. Guillot, J. Lavaud, V. Josserand, J. L. Coll, J. F. Mano, C. Picart, *Acta Biomater.* **2015**, *15*, 139.
[64] S. Goenka, V. Sant, S. Sant, *J. Controlled Release* **2014**, *173*, 75.
[65] J. Li, N. Ren, J. Qiu, X. Mou, H. Liu, *Int. J. Nanomed.* **2013**, *8*, 3415.
[66] M. E. Gomes, R. L. Reis, *Int. Mater. Rev.* **2004**, *49*, 261.
[67] R. L. Reis, J. S. Román, *Biodegradable Systems in Tissue Engineering and Regenerative Medicine*, CRC Press, Boca Raton, FL **2004**.
[68] R. Justin, B. Chen, *Carbohydr. Polym.* **2014**, *103*, 70.
[69] R. Justin, B. Chen, *J. Mater. Chem. B* **2014**, *2*, 3759.
[70] K. P. Menard, *Dynamic Mechanical Analysis: A Practical Introduction*, CRC Press, Boca Raton, FL **2008**.
[71] H. Fan, L. Wang, K. Zhao, N. Li, Z. Shi, Z. Ge, Z. Jin, *Biomacromolecules* **2010**, *11*, 2345.
[72] Y. Pan, T. Wu, H. Bao, L. Li, *Carbohydr. Polym.* **2011**, *83*, 1908.
[73] N. M. Alves, J. L. G. Ribelles, J. A. G. Tejedor, J. F. Mano, *Macromolecules* **2004**, *37*, 3735.
[74] R. L. Reis, D. Cohn, *Polymer Based Systems on Tissue Engineering, Replacement and Regeneration*, Springer, Netherlands **2002**.
[75] C. Wan, B. Chen, *J. Mater. Chem.* **2012**, *22*, 3637.
[76] R. R. Costa, A. M. S. Costa, S. G. Caridade, J. F. Mano, *Chem. Mater.* **2015**, *27*, 7490.
[77] X. Yang, Y. Tu, L. Li, S. Shang, X. Tao, *ACS Appl. Mater. Interfaces* **2010**, *2*, 1707.
[78] R. E. Gorga, R. E. Cohen, *J. Polym. Sci., Part B: Polym. Phys.* **2004**, *42*, 2690.
[79] D. Blond, V. Barron, M Ruether, K. P. Ryan, V. Nicolosi, W. J. Blau, J. N. Coleman, *Adv. Funct. Mater.* **2006**, *16*, 1608.
[80] D. Han, L. Yan, W. Chen, W. Li, *Carbohydr. Polym.* **2011**, *83*, 653.
[81] X. Qi, D. Yan, Z. Jiang, Y. Cao, Z. Yu, F. Yavari, N. Koratkar, *ACS Appl. Mater. Interfaces* **2011**, *3*, 3130.
[82] M. Yoonessi, J. R. Gaier, *ACS Nano* **2010**, *4*, 7211.
[83] N. Yousefi, M. M. Gudarzi, Q. Zheng, S. H. Aboutalebi, F. Sharif, J. Kim, *J. Mater. Chem.* **2012**, *22*, 12709.
[84] W. Li, X. Tang, H. Zhang, Z. Jiang, Z. Yu, X. Du, Y. Mai, *Carbon* **2011**, *49*, 4724.
[85] S. M. Oliveira, N. M. Alves, J. F. Mano, *J. Adhes. Sci. Technol.* **2014**, *28*, 843.
[86] A. L. Hillberg, C. A. Holmes, M. Tabrizian, *Biomaterials* **2009**, *30*, 4463.
[87] C. Picart, R. Elkaim, L. Richert, F. Audoin, Y. Arntz, M. da Silva Cardoso, P. Schaaf, J.-C. Voegel, B. Frisch, *Adv. Funct. Mater.* **2005**, *15*, 83.